Stability Implications of Renewable Energy Integration in Interconnected Power Systems

MABROUKA GHILOUFI*, LASSAAD SBITA
Process Laboratory, Energetic, Environment and Electrical System (PEESE),
National Engineering School of Gabes (ENIG),
University of Gabes,
TUNISIA

*Corresponding Author

Abstract: - This paper investigates the impact of renewable energy source (RES) integration on the small-signal stability of interconnected power systems using linear modal analysis. Unlike conventional synchronous generators, inverter-based RESs are non-dispatchable and do not inherently contribute rotational inertia or governor-based damping. Their increasing penetration consequently degrades system frequency response, leading to a higher rate of change of frequency (RoCoF) and a lower frequency nadir following disturbances. Modal analysis reveals that both interarea and local electromechanical oscillation modes experience reduced damping as RES penetration levels rise. Furthermore, wind power integration introduces a distinct low-frequency interarea oscillatory mode not observed with equivalent photovoltaic (PV) integration. A modified Kundur two-area test system is employed to model these scenarios, wherein wind and solar farms progressively replace conventional synchronous generation to evaluate their influence on system dynamic stability.

Key-Words: - Power system stability -Rate of change of frequency - System inertia - Renewable energy sources- Voltage stability - Rotor angel stability.

Received: May 28, 2025. Revised: January 14, 2026. Accepted: May 13, 2026. Published: July 20, 2026.

1 Introduction

To deal with carbon emissions and climate change, more countries worldwide are turning to renewable energy sources that are moving away from fossil fuels toward clean energy sources like wind and photovoltaic plants, which generate electricity without directly emitting carbon and hence contribute to a sustainable and green energy system. Renewable energy sources, by their very nature, fluctuate in energy output according to weather and environmental factors. However, such fluctuations penetrating the electrical grid change the dynamics considerably. The increasing RESs need to change infrastructure, operating practices, and control policies to face new challenges while ensuring a stable and reliable supply of power.

Modern electrical grids have developed into large-scale and increasingly complex systems because of advances in technology and a growing demand for energy, which has led to a much larger integration of renewable energy sources such as solar and wind power. However, these renewable sources face fundamental challenges. Impediments, not least, the lack of inertia normally provided by traditional systems, [1]. This is because solar power plants lack inertia; their output gets dynamically affected by external drivers such as temperature and solar radiation. This is because they fall under the category of static generation techniques. In the case of wind turbines, even though there is a generator that ensures the conversion of mechanical energy to electrical energy, its rotational speed depends on the wind speed, hence bringing about continuous changes in output power. This condition results in a power generation mismatch, which creates an issue in making the operation of the air turbines in cohesion with that of the grid at the same time hence posing a problem to the integration of the grid, [2]. The stability of the power system together with issues to do with the frequency response, becomes highly contentious in the absence of governor damping and natural inertia. Too little damping may cause the fluctuations in voltage and frequency variations to increase much faster, which would also increase the probability of instability and power outages and may result in harm to the system and its components.

In this work, we present a review to estimate the stability potential of power systems. Among them is the power system strength which measures the ability and restoration capabilities of the system to return all nodal voltages to their specified range under steady-state and after disturbances. We also analyze parameters like Inertia, Rate of Change of Frequency. Those would indeed ease carrying out detailed assessments and comprehension of the dynamic properties of the electrical network and analysis of behavior under diverse aspects. Operators use the indicators to facilitate forecast activities. Meanwhile, operators apply these indicators so they could pinpoint areas subject to vulnerabilities and develop measures leading towards an improvement in grid resilience and overall grid stability.

The purpose of this paper is to investigate the dynamic characteristics of the power system inherent to a massive renewable energy penetration. The dynamic aspects of these production sources connected to the grid will be treated by linear modal analysis. This method will be applied on a bizonal electrical network to treat low frequency, local and interarea oscillations, as well as the impact of renewable energies on the inertia's system and RoCoF.

2 Interconnected Power System

Interconnected power systems are gradually developing keeping pace with the large scale of RES integration into grid particularly wind and solar plants. For example the case of the North American electricity grid (the four giant synchronous system the east, west, Quebec and Texas interconnections) or developing the Maghreb and euro-Mediterranean interconnection like Tunisian grid, as depicted in Figure 1, [3].

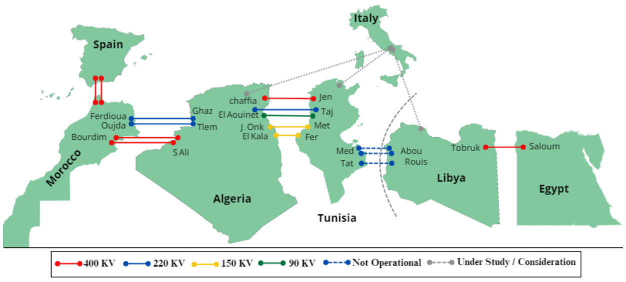

Fig. 1: North Africa grid interconnection
Source: created by the authors

A description of each of the three major grid interconnection types provides context for their respective functions in overall power system integration, [4].

2.1 AC Power System Interconnection

This interconnection is usually through transformer substations, which pair up power grids together, by managing and balancing the voltage accordingly for power supply. The systems react to one another in real time, allowing energy to transfer across the network with minimal interruption.

2.2 DC Power System Interconnection

Here, high-voltage direct current (HVDC) transmission lines are employed in the interconnection of two power systems using converters at both the ends. An AC to DC conversion is made by a rectifier at the sending end, and an inverter at the receiving end converts DC back to AC. The use of electronic control systems on power switches enables control of voltage during steady-state and dynamic operation and thus provides very flexible interconnection between asynchronous systems.

2.3 Hybrid AC/DC Power System Interconnection

The principle involves transmission of both AC and DC and is best suited to large grid systems. The technique takes maximum benefit from the merits of both AC transmission for distribution locally and DC for effective transmission over long distances for improved power system performance and stability.

3 Overview of Power System Issues Associated with RES integration

RES penetration in the electrical grid affects its dynamic and static behaviour particularly the frequency, rotor angle and voltage stability, for massive penetration of wind or photovoltaic plants these effects depend on both the used wind turbine technology and the penetration rate in the electrical network various studies have pointed out that PV and wind generation cause a disturbed regime which can be composed in two regime the transient regime occurs just after integration and the dynamic regime corresponds to slower phenomena and occurs after the transitional period that may last to several minutes, [5]. It can be shown that with a low penetration rate the grid will keep its stable state whereas on the other hand for a high integration of RES the network can result in an instability case, [6].

3.1 Frequency Response with Consideration of RES Integration

Frequency stability is the tendency of a system to return to its original state after some disturbance in the network disturbances, [7]. Normally, it arises owing to some cause which in most cases is identified as reducing system inertia, which is an essential factor for keeping the stability of electrical systems, it tends to enable the network to absorb the frequency deviations happening just after any sudden mismatch between generation and consumption. Normally, due to a generator or a load loss, synchronous inertia can be termed kinetic energy stored in the system, [8], [9].

The swing equation describes the relationship between the correlation between frequency response and rotational inertia of the grid [10], underscoring the critical role of inertia in maintaining grid stability [11].

$$P_m - P_e = \frac{dE_{kinetic}}{dt}$$
$$= \frac{d\left(\frac{1}{2}J\omega^2\right)}{dt} = J\omega\frac{d\omega}{dt} = \frac{2HS_n}{dt}\frac{d\omega}{dt} \quad (1)$$
$$\frac{P_m - P_e}{S_n}\frac{2H}{\omega}\frac{d\omega}{dt}$$

The rated rotor angular speed is denoted by ω (in rad/s); the equivalent kinetic energy of the synchronous generator (SG) is represented by E_K; the moment of inertia is given by J (in kg·m²); the inertia constant of the SG is denoted by H; and the system's rated apparent power is indicated by S_B (in kW).

Generally, the equivalent inertial constant of an electrical system comprising N synchronous machines and M renewable energy sources can be determined by applying the following mathematical relationship:

$$H_{sys} = H_{SG} + H_{RES}$$
$$H_{sys} = \frac{\Sigma_{i=1}^{N} H_{SG,i} * S_{SG,i} + \Sigma_{k=1}^{M} H_{Virtual,k} * S_{RES,k}}{\Sigma_{i=1}^{N} S_{SG,i} + \Sigma_{k=1}^{M} S_{RES,k}} \quad (2)$$

In contrast, renewable energy sources (RES) typically lack inherent rotational inertia and cannot provide an immediate inertial response or release stored kinetic energy following a disturbance. Consequently, the reduced aggregate system inertia exacerbates the RoCoF during grid contingencies, [12]. Elevated RoCoF values intensify transient frequency deviations, resulting in deeper frequency nadirs and more pronounced overshoots. Such severe excursions can trigger the maloperation of under/over-frequency protection relays, leading to unintended circuit breaker tripping and the inadvertent isolation of critical generation or transmission assets. Under severe operating conditions, these unintended disconnections may precipitate cascading failures, potentially culminating in widespread load shedding or complete system blackouts, [13]. The dynamic relationship between active power imbalance and frequency deviation is governed by the swing equation, which can be determined by this formula:

$$RoCoF = \frac{df}{dt}$$
$$= \frac{f}{2E_{kinetic}}\left(P_m - P_e\right) \quad (3)$$
$$= \frac{f}{2E_{kinetic}}\Delta P$$

Figure 2 demonstrates how low-inertia systems suffer sharper frequency drops (Fast RoCoF), deeper nadirs, and larger steady-state offsets compared to high-inertia systems, highlighting the critical role of inertia in stabilizing grid frequency response, [14], [15].

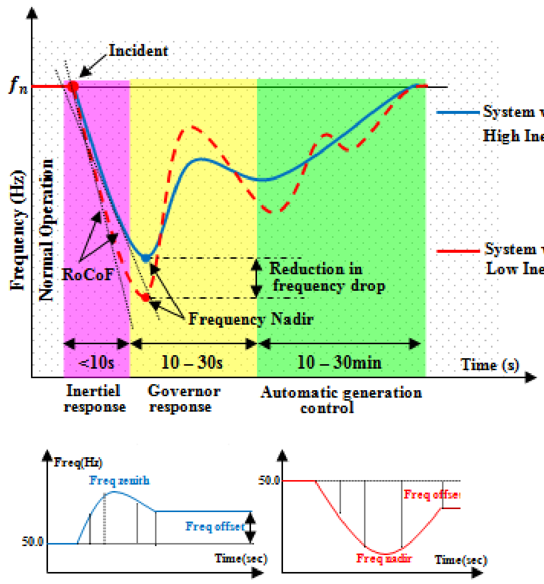

Fig. 2: Effects of low inertia power system on frequency response
Source: created by the authors

3.2 Voltage Stability with Consideration of RES Integration

An electrical grid manifests voltage stability through its capability to keep admissible voltage levels in different bus bars beneath regular working and directly after an intervention or emergency voltage fluctuation [16], which arises mainly when a slight decrease or increase in the voltage in different bus bars until the climax point, is almost reached when voltage dip briskly or energy demand is greater than the network capacity, [17].

Wind power plants are discontinuous in nature and contributing to unexpected voltage fluctuations, if recovery is not done faults can occur large faults can produce voltage volatility. In wind power generators equipped with squirrel cage induction generators (SCIG) when a disturbance occurs the inequality between the mechanical power obtained from the wind and the power supplied to the grid causes the induction generator to accelerate, if the voltage is not restored the wind generator will continue to accelerate and consume a large proportion of reactive power, this causes a voltage drop. Conversely, synchronous generator-type variable-speed wind turbines accelerate voltage recovery after a fault because their exciters increase reactive power production through voltage sags. Additionally, the sensitivity of static converters to fault over currents caused by voltage sags can have a detrimental effect on mains voltage stability. Photovoltaic generation has unique characteristics in voltage and reactive power control, so voltage stability is affected when replacing synchronous generators with photovoltaic plants.

By using a simple electrical system such as a two-bus bars system depicted in Figure 3, we can analyze the basic concept of voltage stability, [18].

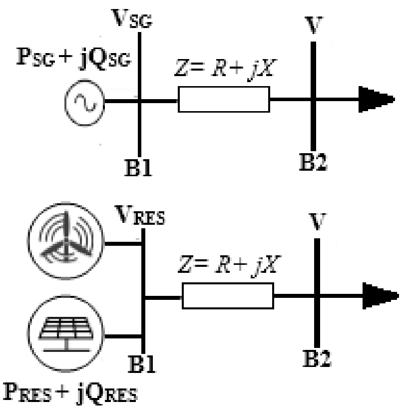

Fig. 3: One line diagram of infinite bus system with a RES power plant
Source: created by the authors

Within the system, the charge is assumed to be of constant power type, the real power move from the sending-end buses (Bus 1 and Bus 2) combines at the intermediate coupling bus (Bus 3) before being transmitted to the receiving-end infinite bus (Bus 4).

– Under conditions of zero renewable energy penetration:

Active power generation exhibits the conventional sinusoidal steady-state behavior characteristic of synchronous machine-dominated systems:

$$P_{SG} = \frac{E_{SG}V}{Z}\sin\delta_{SG} \tag{4}$$

$$Q_{SG} = -\frac{V^2}{Z} + \frac{E_{SG}V}{Z}\cos\delta_{SG} \tag{5}$$

– Under conditions of RES integration:

The following derivations can be expressed:

$$\begin{cases} P_{RES} - \dfrac{V_{RES}^2 R}{R^2 + X^2} = \dfrac{V_{RES}V\left(X\sin\delta - R\cos\delta\right)}{R^2 + X^2} \\ Q_{RES} - \dfrac{V_{RES}^2 X}{R^2 + X^2} = \dfrac{-V_{RES}V\left(\mathrm{R}\sin\delta + X\cos\delta\right)}{R^2 + X^2} \end{cases} \tag{6}$$

$$\begin{gathered} V = V_{RES} - Z * \left(\frac{P_{RES} + jQ_{RES}}{V_{RES}}\right) \\ V = V_{RES} - \left(R + jX\right) * \left(\frac{P_{RES} + jQ_{RES}}{V_{RES}}\right) \end{gathered} \tag{7}$$

Squaring both sides of the preceding equations and summing the resulting terms yields an explicit expression for V_{RES}:

$$\begin{gathered} \left(P_{RES} - \frac{V_{RES}^2 R}{R^2 + X^2}\right)^2 + \left(Q_{RES} - \frac{V_{RES} X}{R^2 + X^2}\right)^2 = \frac{V_{RES}^2 V^2}{R^2 + X^2} \\ V_{RES} = \sqrt{R_{RES}R + Q_{RES}X + \frac{V^2}{2} \pm \sqrt{\left(P_{RES}R + Q_{RES}X + \frac{V^2}{2}\right) - Z^2\left(P_{RES}^2 + Q_{RES}^2\right)}} \\ Z_{RES} = R_{RES} + jX_{RES} = \frac{V_{RES}^2}{-P_{RES} + jQ_{RES}} \end{gathered} \tag{8}$$

The impedance-based index for a distribution system with single-infeed renewable energy integration can be expressed as:

$$\begin{gathered} K_{RES} = \frac{\left|Z_{RES}\right|}{\left|Z\right|} \\ K_{RES} = \frac{V_{RES}^2}{\left|Z\right|\sqrt{P_{RES}^2 + Q_{RES}^2}} \end{gathered} \tag{9}$$

Where |Z| denotes the magnitude of the vector. Based on Equation 6, the system exhibits static voltage stability for $K_{RES} > 1$, reaches critical stability at $K_{RES} = 1$, and becomes voltage-unstable when $K_{RES} < 1$.

A range of tools is employed to estimate voltage stability including but not limited the P-V curve and Q-V curve methods, as illustrated in Figure 4, being among the most common approaches, [19], [20], these two primary techniques are widely applied to predict voltage stability, they are constructed through a sequence of power flow analyses and serve to identify the load limits of a power system, P-V curves in particular are developed by progressively increasing both the real and reactive power loads until a critical voltage threshold is attained, [21].

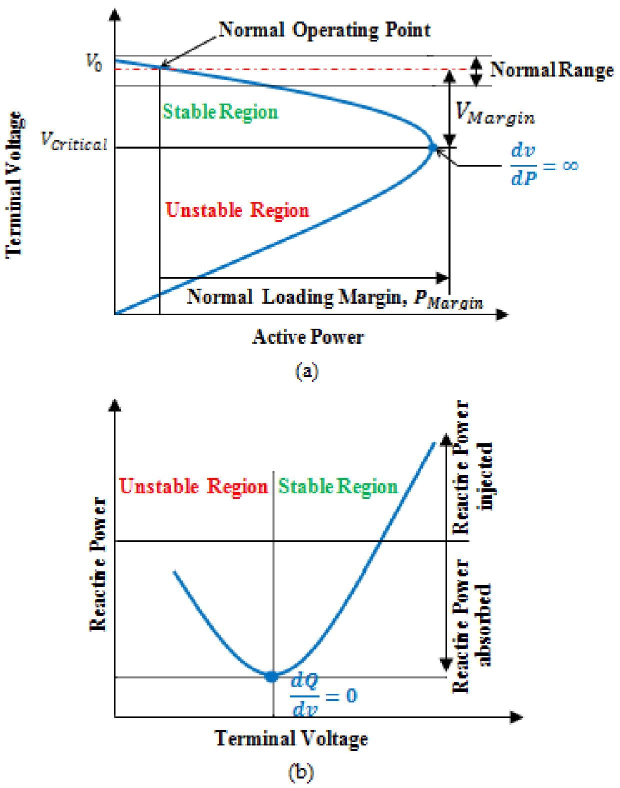

Fig. 4: **(**a) Power voltage (P-V) and (b) Reactive voltage (Q-V) curves for voltage stability analysis
Source: created by the authors

3.3 Rotor Angel Stability with Consideration of RES Integration

Rotor angle stability is the capability of a synchronous machine associated to an electrical grid to remain in synchronization during regular operations conditions and after being subjected to perturbation, the stability problem revolves around analyzing the electromechanical oscillations. Naturally, present in electrical systems at its core the problem arises from how the output of a synchronous machine fluctuates in reaction to rotor oscillations, [9], [22].

The equal area criterion (EAC) is a graphical approach for assessing whether a synchronous machine can regain synchronism after a disturbance such as a sudden increase in load or a fault in the system, it involves a comparison of areas under the power-angle curve representing the power output of the generator as a function of the rotor angle, [18].

The relationship between rotor angle and accelerating power is expressed as follows:

$$\frac{d^2\delta}{dt^2} = \frac{\omega_0}{2H}\left(P_m - P_e\right) \tag{10}$$

As *Pe* is a nonlinear function of δ, the equation resists direct solution. By multiplying both sides by *2dδ/dt*, the expression becomes:

$$2\frac{d\delta}{dt}\frac{d^2\delta}{dt^2} = \frac{\omega_0\left(P_m - P_e\right)}{H}\frac{d\delta}{dt}$$
$$\frac{d}{dt}\left[\frac{d\delta}{dt}\right]^2 = \frac{\omega_0\left(P_m - P_e\right)}{H}\frac{d\delta}{dt} \tag{11}$$
$$\left[\frac{d\delta}{dt}\right]^2 = \int \frac{\omega_0\left(P_m - P_e\right)}{H} d\delta$$

Following a disturbance, the speed deviation *dδ/dt* deviates from its initial zero state. For transient stability, the rotor angle *δ* must remain bounded, implying it reaches a maximum excursion before reversing direction. This physical constraint necessitates that the speed deviation returns to zero at a finite time post-disturbance. The stability criterion is formulated as:

$$\int_{\delta_0}^{\delta_{\max}} \frac{\omega_0}{H}\left(P_m - P_e\right) d\delta = 0 \tag{12}$$

-Pre-fault condition: before the fault, the grid is at a steady-state operating point with an electric network transfer where the mechanical power P_m supplied balances the system P_e.
-During fault: when a three-phase fault happens, the yield of the generators electrical grid drops to nearly zero because the power failure reduces the effective power transfer capability to almost zero.
-Post-fault condition: once the fault is cleared, the system returns to a new operating condition the network is usually less than $P_e$because of variations in system impedance or configuration.

Stability can be determined by comparing two areas on this graph for the network to keep stable (A1=A2). If (A1 > A2), the grid will lose synchronism because the rotor will accelerate beyond control. The energy gained is:

$$A1 = A_{Acceleration} = \int_{\delta_0}^{\delta_{cr}} \left(P_m - P_e\right) d\delta \tag{13}$$

The energy lost during deceleration as δ changes from *δ1* to *δm* is given by:

$$A2 = A_{Deceleration} = \int_{\delta_{cr}}^{\delta_{max}} \left(P_e - P_m\right) d\delta \qquad (14)$$

In the context of transient stability analysis based on the equal-area criterion EAC illustrated in Figure 5, the critical clearing angle (CCA), denoted as δcc , and its corresponding critical clearing time (CCT), denoted as tcc , constitute fundamental metrics for assessing the maximum permissible fault duration prior to irreversible loss of synchronism. Specifically, the CCA represents the maximum rotor angle deviation at which a fault must be cleared to ensure that the accelerating area does not exceed the available decelerating area, thereby preserving post-fault stability. The CCT, in turn, denotes the temporal equivalent of the CCA. Mathematically, under the classical swing equation framework, these quantities can be expressed as follows:

$$\delta_{cr} = \frac{\omega_0 P_m}{4H} + t_{cr}^2 \delta_0 \qquad (15)$$

$$t_{cr} = \sqrt{\frac{4H\left(\delta_{cr} - \delta_0\right)}{\omega_0 P_m}} \qquad (16)$$

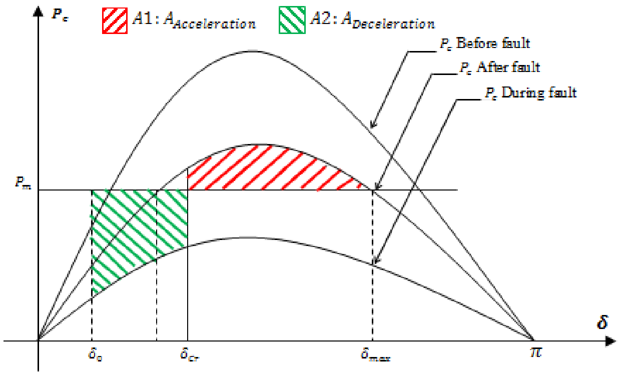

Fig. 5: Equal Area Criterion for a Three-Phase Fault in Power System
Source: created by the authors

Transient stability addresses large disturbances causing significant rotor speed, angle, and power fluctuations, typically unfolding within seconds in RES-integrated power systems. Rotor angle stability analysis relies on key assumptions: balanced three-phase conditions, small frequency deviations from synchronism, and steady-state network/impedance loads. During short circuits, high-frequency currents appear in generators, while voltages, currents, and powers remain computable via standard power flow equations.

Small-signal stability refers to a power system's ability to maintain synchronism under minor disturbances, such as small load switching or line tripping, which can otherwise trigger sustained oscillations.

The oscillation modes arise: local modes (0.8 to 2 Hz), involving single or co-located generators, and inter-area modes (0.1 to 0.8 Hz), where generator groups in different areas oscillate against each other, [6].

Notably, wind turbine integration can introduce novel inter-area oscillation patterns, further complicating small-signal stability assessment in renewable-rich grids. Wind turbines retain mechanical rotational dynamics coupled with multi-loop converter controls, creating electromechanical–electromagnetic interactions that can shift mode shapes, reduce damping, or generate new low-frequency coupling between distant generator groups. Photovoltaic systems are purely inverter-based with no rotating mass; their dynamics are dominated by fast current/voltage regulation and DC-link control, which typically only modulate or damp an existing dominant inter-area mode through power redistribution or PLL interactions rather than creating new coupling pathways. Consequently, WTs often introduce novel inter-area oscillation patterns, whereas PV integration typically influences only one primary inter-area mode.

4 Description of the Studied Power Systems

4.1 Kundur Two Areas Power System

The network used for the study in Figure 6 is a four generator and 11 node system. It has a two symmetrical area structure. In each of these areas, two generators and two load buses are placed. An interconnect bus connects all these. Importantly, this network is composed of fully equivalent generators with a rated capacity of 900 kVA connected to an operational voltage of 20 Kv, [6], [23].

A photovoltaic system (PV) is connected to Area 1 at Bus 6, and a wind farm (WT) is connected to Area 2 at Bus 10, each connected to the grid through a transformer and a line Impedance Z = j0.001 p.u., as shown in Figure 6. The wind speed model is based on a Weibull distribution with a scale parameter of c = 2 and a shape parameter of k = 9. The rated power of each wind turbine is 2 MW. Table 1 shows that the increase in renewable generation is offset by a decrease in synchronous generator output. This reduction in generation corresponds to a decrease in their scheduled active power operating point, and consequently, the equivalent system inertia decreases proportionally.

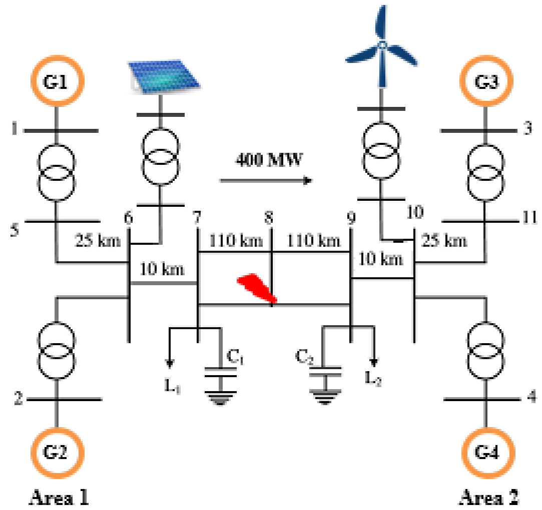

Fig. 6: Single-line diagram of the Kundur test system integrating photovoltaic and wind farms
Source: created by the authors

Table 1 shows the static state of the network before the integration of the renewable energy. The network has symmetry in both production and loading areas while the G4 generator serving as the balance node.

Table 1. The static state of Kundur

Bus	V	Phase	P_g	Q_g	P_L	Q_L
01	1,03	0,3533	7	1,8245	0	0
02	1,01	0,1830	7	2,2843	0	0
03	1,03	-0,1186	7,1890	1,7242	0	0
04	1,01	-0,2963	7	1,9355	0	0
05	1,0068	0,2406	0	0	0	0
06	0,9791	0,0648	0	0	0	0
07	0,9628	-0,0815	0	0	9,67	-1
08	0,9482	-0,3231	0	0	0	0
09	0,9738	-0,5602	0	0	17,67	-2,5
10	0,9848	-0,4138	0	0	0	0
11	1,0088	-0,234	0	0	0	0

Source: created by the authors

Table 2 presents the active power generation dispatch for the synchronous generators (G1–G4) and renewable energy sources (PV and WT) across varying levels of RES penetration. The data is categorized by control area (Area 1 and Area 2) and expressed in per-unit (pu) values. The scenarios range from a 0% RES penetration Base Case (B.C.) to a high penetration level of 60%. As illustrated in the table, increasing RES penetration results in a corresponding reduction in the output of conventional synchronous generators to accommodate the rising contribution from PV and wind turbine units.

Table 2. Active power output of synchronous generators PV, and WT for various res penetration scenarios

RES Penetration (%)	Active Power Generation (pu)					
	Area 1			Area 2		
	PV	G1	G2	WT	G3	G4
0% (B.C)	0	7	7	0	7.1902	7
10%	1.4	6.3	6.3	1.4	6.490	6.3
20%	2.8	5.6	5.6	2.8	5.791	5.6
40%	5.6	4.2	4.2	5.6	4.386	4.2
60%	8.4	2.8	2.8	8.4	2.9	2.8

Source: created by the authors

4.2 Stability Analysis with Consideration of RES Integration

This subsection investigates the dynamic response of the point of interconnection (POI) voltage of the renewable energy source as a function of the available fault level, the power injected by the inverter-based RES , and its location within the network, [24], [25]. The complex AC power output of the RES, defined as $RES=P_{RES}+jQ_{RES}$, is expressed in the synchronous *d-q* reference frame as follows:

$$P_{RES}=\frac{3}{2}\left(V_{RES,d}*I_{RES,d}+V_{RES,q}*I_{RES,q}\right)$$
$$Q_{RES}=\frac{3}{2}\left(V_{RES,q}*I_{RES,d}+V_{RES,d}*I_{RES,q}\right) \quad (17)$$

Linearization of the preceding equations results in the following differential relationship among the incremental changes in the RES terminal voltage $\Delta V_{RES,d}$ and $\Delta V_{RES,q}$, current $\Delta I_{RES,d}$ and $\Delta I_{RES,q}$, and output power ΔP_{RES} and ΔQ_{RES}:

$$\Delta P_{RES}=\frac{3}{2}\begin{pmatrix}V_{RES,d}*\Delta I_{RES,d}\\+I_{RES,d}*\Delta V_{RES,d}\\+V_{RES,q}*\Delta I_{RES,q}\\+I_{RES,q}*\Delta V_{RES,q}\end{pmatrix}$$
$$\Delta Q_{RES}=\frac{3}{2}\begin{pmatrix}V_{RES,q}*\Delta I_{RES,d}\\+I_{RES,d}*\Delta V_{RES,q}\\-V_{RES,d}*\Delta I_{RES,q}\\-I_{RES,q}*\Delta V_{RES,d}\end{pmatrix} \quad (18)$$

By rearranging equation (18), the voltage deviations $\Delta V_{RES,d}$ and $\Delta V_{RES,q}$ can be expressed in terms of ΔP_{RES} , ΔQ_{RES} , $\Delta I_{RES,d}$, and $\Delta I_{RES,q}$ as follows:

$$\Delta V_{RES,d} = \begin{pmatrix} a\Delta P_{RES} - b\Delta Q_{RES} \\ -c\Delta I_{RES,d} - d\Delta I_{RES,q} \end{pmatrix}$$
$$\Delta V_{RES,q} = \begin{pmatrix} b\Delta P_{RES} + p\Delta Q_{RES} \\ -q\Delta I_{RES,d} - r\Delta I_{RES,q} \end{pmatrix} \tag{19}$$

The resulting state-space model is given by [26]:

$$\begin{aligned} \Delta\dot{x} &= A\Delta x + B\Delta u \\ \Delta y &= C\Delta x + D\Delta u \end{aligned} \tag{20}$$

Where the state vector $\Delta x = \begin{bmatrix} \Delta I_{RES,d} \\ \Delta I_{RES,q} \\ \Delta V_{POI,d} \\ \Delta V_{POI,q} \\ \Delta I_{POI,d} \\ \Delta I_{POI,q} \end{bmatrix}$,

Input vector $\Delta u = \begin{bmatrix} \Delta P_{RES} & \Delta Q_{RES} \end{bmatrix}^T$

The state and input matrices are

$$A = \begin{bmatrix} -\frac{\alpha_1}{L_f} & \alpha_2 & 0 & 0 & -\frac{1}{L_f} & 0 \\ -\alpha_3 & -\frac{\alpha_4}{L_f} & 0 & 0 & 0 & -\frac{1}{L_f} \\ 0 & 0 & -\frac{R_s}{L_s} & \omega_0 & \frac{1}{L_s} & 0 \\ 0 & 0 & -\omega_0 & -\frac{R_s}{L_s} & 0 & \frac{1}{L_s} \\ \frac{1}{C_f} & 0 & -\frac{1}{C_f} & 0 & 0 & -\omega_0 \\ 0 & \frac{1}{C_f} & 0 & -\frac{1}{C_f} & \omega_0 & 0 \end{bmatrix}$$

And $B = \begin{bmatrix} B_1 & B_2 \end{bmatrix}$

Where

$$B_1 = \left[\frac{a}{L_f}, \frac{b}{L_f}, 0,0,0,0\right]^T \quad B_2 = \left[-\frac{b}{L_f}, \frac{p}{L_f}, 0,0,0,0\right]^T$$

$$\alpha_1 = \left(R_f + c\right) \qquad \alpha_2 = \left(\omega_0 - \frac{d}{L_f}\right)$$

$$\alpha_3 = \left(\omega_0 + \frac{q}{L_f}\right) \qquad \alpha_4 = \left(R_f + r\right)$$

The point-of-interconnection voltage magnitude is selected as the system output. Accordingly, the output equation of the linearized state-space model is expressed as:

$$\begin{aligned} \Delta y &= C\Delta x + D\Delta u \\ \Delta y &= \Delta\left|V_{POI}\right| = C\Delta X \end{aligned} \tag{21}$$

Where $C = \left[0, 0, \frac{V_{POI,d}}{\left|V_{POI}\right|}, \frac{V_{POI,q}}{\left|V_{POI}\right|}, 0, 0 \right]$

The mode associated with an eigenvalue λ_I shows time-dependent behavior, resolved by $e^{\lambda_i t}$. As a result, eigenvalues have a significant impact on power system stability. A real eigenvalue correlate to a non-oscillatory mode. If the real eigenvalue is negative, the mode decays at a faster pace as the magnitude grows. On the other hand, a positive real eigenvalue suggests periodic instability. When complex eigenvalues appear in conjugate pairs, each pair denotes an oscillatory mode. The real component of the eigenvalue dictates the damping effect, whereas the imaginary part affects the oscillation frequency, [27], [28]:

$$\lambda = \sigma \pm j\omega \tag{22}$$

In Hertz, the frequency of the oscillation is defined:

$$f = \frac{\omega}{2\pi} \tag{23}$$

In this way, the damping ratio is given:

$$\zeta = -\frac{\sigma}{|\lambda|} = -\frac{\sigma}{\sqrt{\sigma^2 + \omega^2}} \tag{24}$$

5 Simulation Results

5.1 Eigenvalue and Stability

Renewable energy integration into the test system leads to a reduced inertial contribution of synchronous machines, which reduces their damping rate nevertheless higher RES penetration into the test system constitutes a possible issue to system stability. Figure 7 shows eigenvalues for 60% levels of res penetration notably the presence of positive eigenvalues indicates instability within the system.

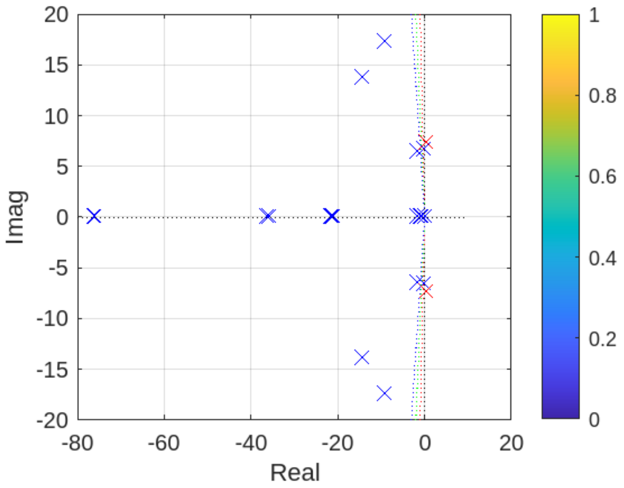

Fig. 7: Eigenvalue trajectories for 60% penetration levels
Source: created by the authors

5.2 Rotor Angel Stability and Inter-Area Oscillation Damping

Linear modal analysis is carried out on the Kundur network without RES. Based on the modal frequency analysis three modes are identified: two local modes and an interarea mode:
-Local Mode 1: It shows the oscillatory action of generator G1 relative to generator G2 within area 1 boundaries.
-Local Mode 2: It shows the oscillation of generator G3 relative to generator G4 within area 2 boundaries.
-Interarea Mode: It describes the oscillatory characteristics of the generators in area 1 relative to those in area.

The mode shape for the inter-area mode is presented in Figure 8.

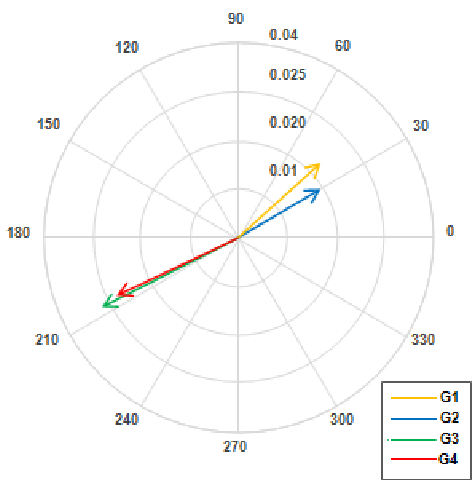

Fig. 8: Mode shape for the inter-area mode
Source: created by the authors

Table 3 shows the linear modal analysis results of the Kundur test system: the linear frequency interarea mode 0.49Hz, and the local frequency modes 0.984 Hz and 0.959 Hz without renewable energy, [29].

Table 3. State matrix eigenvalues for Kundur test system without RES

Eignevalue	Damping	Frequency	Oscillation mode
-0,35803 ±3,11666	0.1156	0,49603184	Interarea mode
-0,80508 ±6,20135	0.1309	0.98487550	Local Mode 1
-0,69865 ±6,02697	0.1168	0.95922206	Local Mode 2

Source: created by the authors

Table 4 presents the result of linear modal analysis conducted. As can be observed, a new interarea mode exists at 0.17 Hz frequency with higher damping compared to the interarea mode that exists when there is no RES, which has a frequency of 0.49 Hz. Raising the integration rate of RES, however, results in reduction of damping of the modes until it leads to negative damping at a 60% integration rate.

Table 4. Kundur network oscillation modes integrating the RES

Case	Eigenvalue	Damping	Frequency	Oscillation mode
10% RES	-0,27689±3,29761	0.0843	0.52483093	Interarea Mode
	-0,45423±1,09035	0.4582	0.17353459	Interarea Mode
	-0,807045±6,1925	0.1314	0.98558130	Locale Mode 1
60% RES	-0,30083±3,25904	-0.0919	0.51869312	Interarea Mode
	-0,36912±2,75460	0.1352	0.43840900	Interarea Mode
	-0,808545±6,1933	0.1316	0.98569430	Locale Mode 1

Source: created by the authors

The angular speed responses of the four generators are depicted in Figure 9 for two renewable penetration cases: (a) 10% and (b) 40%. Comparison of the two cases reveals that the higher penetration level (40%) results in increased oscillation magnitude during the transient period and less effective damping, with oscillations persisting for a longer duration before reaching steady-state equilibrium.

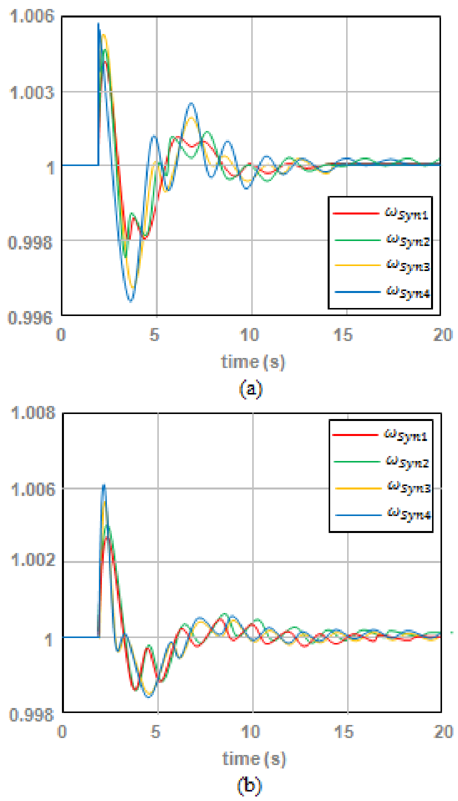

Fig. 9: Angular speed responses: (a) 10% RES penetration; (b) 40% RES penetration
Source: created by the authors

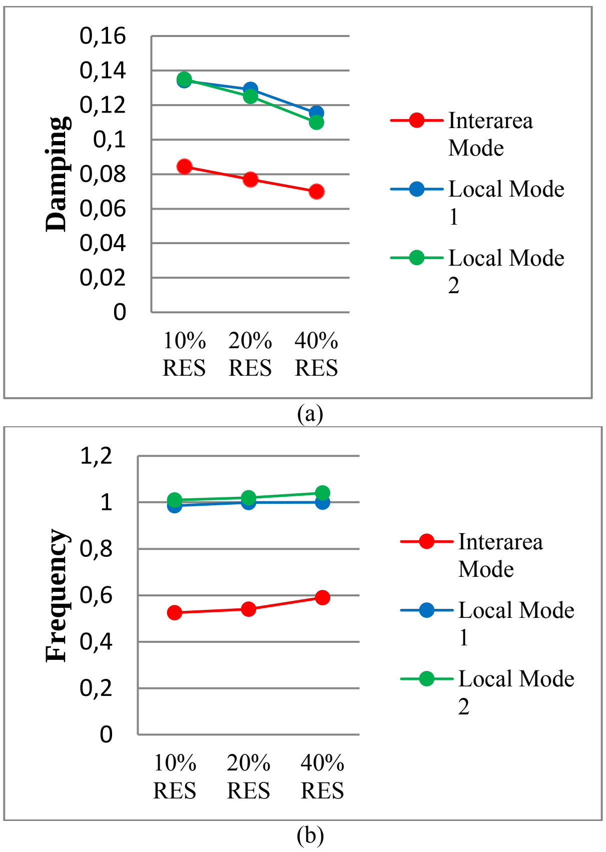

Fig. 10: Variation of (a) Damping and (b) Frequency with RES Penetration Level
Source: created by the authors

Figure 10 depicts the important influence of RES on damping and mode frequency affecting both inter-area and local modes, as the contribution of renewable energy increases the frequency of these modes rises accompanied by a reduction in their damping, efficiency this phenomenon aligns with the observed attrition in the networks equivalent inertia which is directly attributed to the increased integration of renewable energy production, [30].

5.3 Frequency Stability: System Inertia and RoCoF

Renewable energy sources based on solar and wind energy are supplied to the grid by power electronic converters. These converters work to isolate renewable energy production from grid frequency fluctuation, hence making them incapable of stabilizing the grid in case of frequency fluctuation or adding system inertia. Traditional power generators, however, use rotating masses that store kinetic energy, hence imparting natural inertia to the system. Since solar power plants are fixed systems of power generation, they do not necessarily have the capability of imparting inertia. Wind turbines, on the other hand, generate electricity through spinning blades attached to an inertial-type generator, [31]. However, such inertia cannot be transferred to the electric grid in a smooth manner due to differences in the turn rate of turbines caused by asymmetrical wind conditions. Hence, solar and wind power stations, due to their different modes of operation, have it difficult to offer inertia support to the electric power system.

Table 5 shows that the increase in renewable generation is balanced by an equal decline in system inertia.

Table 5. Inertia constants of synchronous generators in area 1 and area 2 under different RES penetration levels

RES Penetration (%)	Inertia H			
	Area 1		Area 2	
	G1	G2	G3	G4
Basic case (0% RES)	6.5	6.5	6.175	6.175
10% RES	5.85	5.85	5.73	5.56
20% RES	5.2	5.2	5.11	4.94
40% RES	3.9	3.9	3.87	3.71
60% RES	2.6	2.6	2.63	2.47

Source: created by the authors

Figure 11 demonstrates that the high renewable energy integration leads to a reduction of inertia constant, this decline leads to faster RoCoF and more significant frequency deviations.

For instance in the case of 40% renewable energy penetration the system exhibits the fastest RoCoF and the frequency nadir drops more compared to other penetration levels. We can conclude that lower system inertia constant accelerates the RoCoF and amplifies deviations from nominal frequency values, thereby increasing the risk of grid instability, [32], [33].

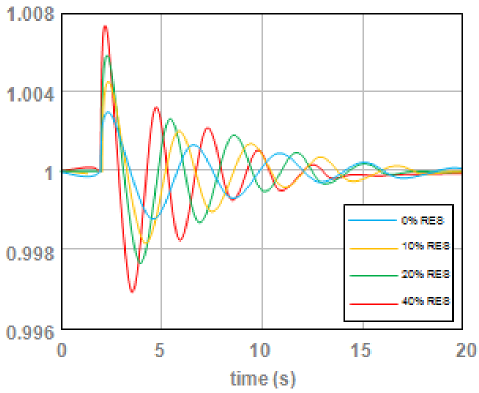

Fig. 11: Frequency response for kundur test system integrating various levels of RES rate
Source: created by the authors

5.4 Voltage Profile

The power output of wind turbines is inherently dependent on the distribution of wind speed. Under low-wind conditions, turbine generation may fall below required thresholds, while high-wind regimes can lead to overproduction, necessitating curtailment or grid support measures. Similarly, photovoltaic generation is subject to diurnal and seasonal variability. These stochastic characteristics introduce rapid and unpredictable fluctuations in active power injection, which can challenge voltage regulation and compromise steady-state stability, particularly in distribution grid with high integration of inverter-based resources. Power systems are designed to operate efficiently under stable voltage profiles; however, the intermittent nature of renewable energy sources can induce significant voltage deviations. In weakly interconnected or lightly loaded networks, such deviations may manifest as sustained oscillations or transient instability, thereby increasing the burden on voltage control mechanisms. Figure 12 presents the steady-state voltage magnitude and phase angle profiles, alongside real and reactive power flows at each busbar. The voltage magnitudes remain within acceptable limits, though localized variations reflect the influence of distributed generation and load patterns. Reactive power injections exhibit pronounced spatial heterogeneity, indicating potential stress on local voltage regulation capabilities.

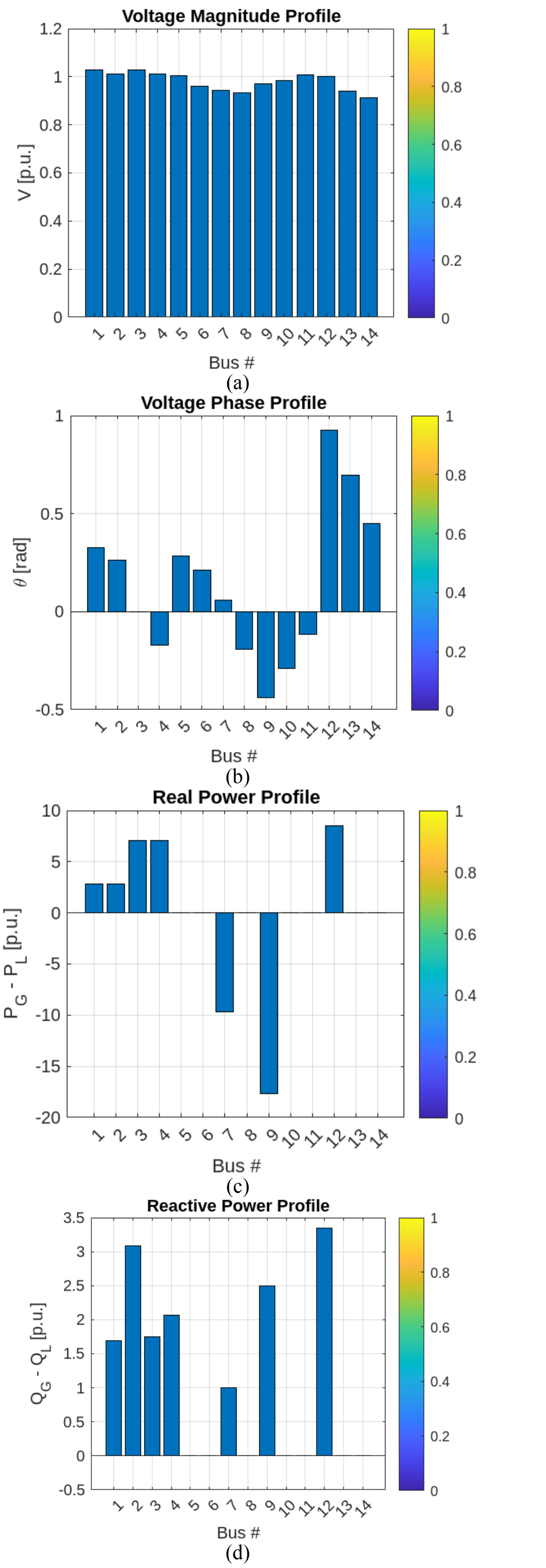

Fig.12: (a) Voltage magnitude profile, (b) Voltage phase profile, (c) Real power profile, and (d) reactive power profile
Source: created by the authors

Figure 13 depicts the terminal voltage responses of the four synchronous generators following a disturbance. The plots reveal initial transients followed by convergence toward new equilibrium points, with Generator 1 exhibiting the most pronounced overshoot due to its proximity to the disturbance source. The damping characteristics suggest that, despite high renewable penetration, the system retains sufficient synchronizing torque to stabilize post-disturbance dynamics, provided that conventional generators remain online and contribute inertial and reactive support. These results underscore the critical role of synchronous machines in maintaining voltage stability under high-renewable scenarios, even when operated near minimum loading. Strategic deployment of grid-forming inverters or dynamic reactive compensation may further enhance resilience, particularly in systems transitioning toward inverter-dominated architectures.

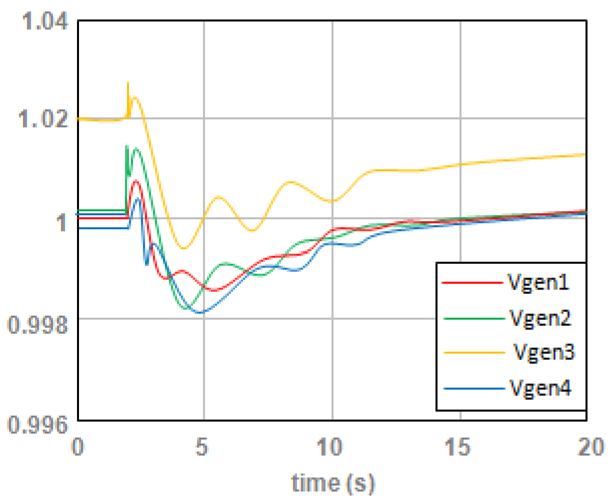

Fig. 13: Terminal voltage responses of the four generators
Source: created by the authors

6 Conclusion

This work presents a comparative analysis of the Kundur two-area test system augmented with photovoltaic (PV) and wind energy sources under increasing levels of instantaneous renewable penetration. Linear modal analysis of the modified bizonal network yields the following key observations:

- The integration of a doubly-fed induction generator (DFIG)-based wind farm introduces an additional oscillatory mode in the interarea dynamics of the system.
- In contrast, the incorporation of PV generation does not produce a new interarea oscillatory mode.
- Increasing the combined penetration level of PV and wind generation reduces modal damping, eventually resulting in negative damping and consequent degradation of system stability.
- At high instantaneous penetration levels of inverter-based resources, maintaining synchronous generators in operation, even at minimum MW output, can enhance damping of electromechanical oscillations and contribute to overall system stability.

References:

[1] Amil Daraz, Hasan Alrajhi, Ahmed N. M. Alahmadi, Mohit Bajaj, Abdul Rahman Afzal, Guoqiang Zhang and Kunpeng Xu, Frequency stabilization of interconnected diverse power systems with integration of renewable energies and energy storage systems, *Scientific Reports*, Vol.14, No.1, 2024, pp. 25655. DOI: 10.1038/s41598-024-76980-z.

[2] Engr. Dr. Badar Ul Islam, Zuhairi Baharudin, and Parameshwari Kattel, Inertia Theory Frequency Dynamic Analysis and Control of Power System with High Proportion of Renewable Source, *Mathematical Problems in Engineering*, Vol. 2021, No. 1, pp. 9472957. DOI: 10.1155/2021/9472957.

[3] Kenza Kilani, Adnene Haj Hamida, and Mohamed Elleuch, North Africa grid interconnection weakness: Impact on the Tunisian PES emergencies, *Energy Reports*, Vol.5, 2019, pp. 1420-1425. DOI: 10.1016/j.egyr.2019.06.010.

[4] Imdadullah, Basem Alamri, Md. Alamgir Hossain, and M. S. Jamil Asghar, Electric Power Network Interconnection: A Review on Current Status, Future Prospects and Research Direction, *Electronics*, Vol. 10, No. 17, 2021, pp. 2179. DOI: 10.3390/electronics10172179.

[5] ECIGRE, *Power Systems With Dispersed Generation:Technologies, Impacts on Development, Operation and Performances. Athens*, Greece, 2005.

[6] Prabha Kundur, *Power System Stability and Control*, McGraw-Hill, 1994.

[7] Erik Orum, Mikko Kuivaniemi, Minna Laasonen, Alf Ivar Bruseth, Erik Alexander Jansson, Anders Danell, Katherine Elkington, and Niklas Modig, *Future system inertia*, European Network of Transmission System Operators for Electricity (entsoe).

[8] Francisco Gonzalez-Longatt, Juan Manuel Roldan-Fernandez, Harold R. Chamorro, Santiago Arnaltes, and Jose Luis Rodriguez-

Amenedo, Investigation of Inertia Response and Rate of Change of Frequency in Low Rotational Inertial Scenario of Synchronous Dominated System, *Electronics*, Vol. 10, No.18, 2021, pp. 2288. DOI: 10.3390/electronics10182288.

[9] Mohammadali Hayerikhiyavi, and Aleksandar Dimitrovski, A Practical Assessment of the Power Grid Inertia Constant Using PMUs, *North American Power Symposium (NAPS)*, Tempe, AZ, USA, 2021, pp. 1-5. DOI: 10.1109/NAPS50074.2021.9449705.

[10] Hormaz Amrolia, Santosh C Vora, Understanding Frequency Response of Induction Motor Winding through Electromagnetic Wave Equations, Advances in Electrical and Electronic Engineering, Vol. 21, No. 3, 2023, pp. 216-225. DOI: 10.15598/aeee.v21i3.5029.

[11] Changjun He, Hua Geng, Kaushik Rajashekara, Ambrish Chandra, Analysis and Control of Frequency Stability in Low-Inertia Power Systems: A Review, *IEEE/CAA Journal of Automatica Sinica*, Vol. 11, No. 12, 2024, pp. 2363-2383. DOI: 10.1109/JAS.2024.125013.

[12] Joseph Shin, Suhyeon Han, Sejin Lee, and Youngsung Kwon, Modified Variable Droop Control Strategy for Improved Primary Frequency Response in Wind Turbine Generators using ROCOF, *Journal of Electrical Engineering and Technology*, Vol.19, No.2, 2024, pp.993–1003. DOI: 10.1007/s42835-023-01592-y.

[13] Alija Mujcinagic, Mirza Kusljugic, and Emir Nukic, Wind Inertial Response Based on the Center of Inertia Frequency of a Control Area, *Energies*, Vol. 13, No.23, 2020, pp. 6177. DOI: 10.3390/en13236177.

[14] Akm Kamrul Hasan, Mohammed H. Haque, Syed Mahfuzul Aziz ,Enhancing Frequency Response Characteristics of Low Inertia Power Systems Using Battery Energy Storage, *IEEE Access*, Vol. 12, 2024, pp. 116861 – 116874. DOI: 10.1109/ACCESS.2024.3444330.

[15] Ghiloufi Mabrouka, Lassaad Sbita, Human-Machine Interaction in Virtual Inertia Control for Smart Grids, Bridging Human-Machine Interaction for Energy Infrastructure, *IGI Global Scientific Publishing*, 2026, pp. 191-232. DOI: 10.4018/979-8-3373-5621-1.ch007.

[16] Lin Yu, Huadong Sun, Shiyun Xu, Bing Zhao, and Jian Zhang, A Critical System Strength Evaluation of a Power System with High Penetration of Renewable Energy Generations, *CSEE Journal of Power and Energy System*, Vol. 8, No.3, 2022, pp. 710-720. DOI: 10.17775/CSEEJPES.2021.03020.

[17] Salah Mokred, Yifei Wang, and Tiancong Chen, A novel collapse prediction index for voltage stability analysis and contingency ranking in power systems, *Protection and Control of Moderm Power Systems*, Vol. 8, No.1, 2023, pp.1-27. DOI: 10.1186/s41601-023-00279-w.

[18] Kenneth Eloghene Okedu, *Introductory Chapter: Power System Stability*, intechopen, 2019. DOI: 10.5772/intechopen.84497.

[19] Viktor Rrotani, Rajmonda Bualoti, Marialis Celo, Static voltage stability analysis with the integration of distributed generation: An albanian case study, *WSEAS Transactions on Power Systems*, Vol. 19, 2024, pp. 427-437. DOI: 10.37394/232016.2024.19.37.

[20] A.S. Ravi, Ashutosh Dwivedi, and Bhuvan Sharma, Voltage Stability Analysis, *International Journal of Scientific and Engineering Research*, Vol. 4, No.6, 2013, pp. 2229-5518.

[21] Bahram Shakerighadi, Farrokh Aminifar, and Saeed Afsharnia, Power systems wide-area voltage stability assessment considering dissimilar load variations and credible contingencies, *Journal of Modern Power Systems and Clean Energy*, Vol. 7, No.3, 2019, pp.78–87. DOI: 10.1007/s40565-018-0420-6.

[22] Selwa Fetissi, Djamel Labed, and Imen Labed, The Transient Stability Study of a Synchronous Generator Based on the Rotor Angle Stability, International Journal of Electrical and Computer Engineering (IJECE), Vol. 5, No.6, 2015, pp. 1319-1327. DOI: 10.11591/ijece.v5i6.pp1319-1327.

[23] Ghiloufi Mabrouka, Lassaad Sbita, Stability of Power Systems Integrating Renewable Energy: Modal Analysis of Linear Dynamic Systems, Modeling, Analysis, and Control of Smart Energy Systems. *IGI Global Scientific Publishing*, 2024. 285-308. DOI: 10.4018/979-8-3693-2999-3.ch014.

[24] M. I. Saleem, Sajeeb Saha, Stability assessment of inverter-based renewable energy sources integrated to weak grids, *IET Energy Systems Integration*, Vol. 6, No. 4, 2024, pp. 525-544. DOI: 10.1049/esi2.12151.

[25] Ghiloufi Mabrouka, Lassaad Sbita, Grid-Forming and Grid-Following Inverters for Virtual Inertia Emulation in Smart Grid, *2025*

IEEE 4th International Conference on Signal, Control and Communication (SCC), IEEE, Sousse, Tunisia , 2025, pp.1-5. DOI: 10.1109/SCC66964.2025.11424851.

[26] E. S. Ali, Sahar M. Abd-Elazim, Power system stability enhancement via new coordinated design of PSSs and SVC, *WSEAS Transactions on Power Systems*, Vol. 9, 2014, pp. 428-438.

[27] F. R. Islam, Avneel Lallu, Kabir Al Mamun, Krishneel Prakash, Impact of wind generators in power system stability, *WSEAS Transactions on Power Systems*, Vol. 13, No. 20, 2018, pp. 235-248.

[28] Federico Milano, *Power System Analysis Toolbox Documentation for PSAT*, University College Dublin, 2013.

[29] M. Klein, G. Rogers, and Prabha Kundur, A fundamental study of inter-area oscillations in power systems, *IEEE Transactions on Power Systems*, Vol. 6, No.3, 1991, pp.914-921. DOI: 10.1109/59.119229.

[30] Charalambos Konstantinou, A Study on the Impact of Wind Generation on the Stability of Electromechanical Oscillations, *arXiv Systems and Control*, 2015. DOI: 10.48550/arXiv.1502.00215.

[31] Sayantan Chowdhury, Ayantika Guria, and Ayantika Guria, Accuracy of Inertia Estimation Method of Two Standard Electrical Power Networks Using Frequency Measurement-Based Method, *Recent Advances in Power Systems*, 2025, pp. 219-236. DOI: 10.1007/978-981-97-7921-5_16.

[32] Salem Alshahrani, Khalid Abdullah Khan, Mohammad Abido, and Muhammad Khalid, Grid-Forming Converter and Stability Aspects of Renewable-Based Low-Inertia Power Networks: Modern Trends and Challenges, *Arabian Journal for Science and Engineering*, Vol. 49, No.11, 2024, pp. 6187–6216. DOI: 10.1007/s13369-023-08399-z.

[33] Bora Çavdar, Omur Akyazi, Erdinc Sahin, and F.M. Nuroglu, Effect of PV Plant on Frequency Stability in IEEE12 Bus System for Different Penetration Levels and Depth of Frequency Support, *Arabian Journal for Science and Engineering*, Vol. 49, No.12, 2024, pp. 15899–15916. DOI: 10.1007/s13369-024-08733-z.

Contribution of Individual Authors to the Creation of a Scientific Article (Ghostwriting Policy)

The authors equally contributed to the present research, at all stages from the formulation of the problem to the final findings and solution.

Sources of Funding for Research Presented in a Scientific Article or Scientific Article Itself

No funding was received for conducting this study.

Conflict of Interest

The authors have no conflicts of interest to declare.